



## Article

# Effect of Copper Doping on Electronic Structure and Optical Absorption of Cd<sub>33</sub>Se<sub>33</sub> Quantum Dots

Fengai Zhao <sup>1</sup>, Shuanglin Hu <sup>1,\*</sup>, Canhui Xu <sup>1</sup>, Haiyan Xiao <sup>2</sup>, Xiaosong Zhou <sup>1</sup>, Xiaotao Zu <sup>2</sup> and Shuming Peng <sup>1,\*</sup>

<sup>1</sup> Institute of Nuclear Physics and Chemistry, China Academy of Engineering Physics, Mianyang 621900, China; fengaizh0506@163.com (F.Z.); xuch1209@caep.cn (C.X.); zlx577@126.com (X.Z.)

<sup>2</sup> School of Physics, University of Electronic Science and Technology of China, Chengdu 610054, China; hyxiao@uestc.edu.cn (H.X.); xtzu@uestc.edu.cn (X.Z.)

\* Correspondence: hushuanglin@caep.cn (S.H.); pengshuming@caep.cn (S.P.); Tel.: +86-28-2496710 (S.H.); +86-28-2496715 (S.P.)

**Abstract:** The photophysical properties of Cu-doped CdSe quantum dots (QDs) can be affected by the oxidation state of Cu impurity, but disagreement still exists on the Cu oxidation state (+1 or +2) in these QDs, which is debated and poorly understood for many years. In this work, by using density functional theory (DFT)-based calculations with the Heyd–Scuseria–Ernzerhof (HSE) screened hybrid functional, we clearly demonstrate that the incorporation of Cu dopants into the surface of the magic sized Cd<sub>33</sub>Se<sub>33</sub> QD leads to non-magnetic Cu 3d orbitals distribution and Cu<sup>+1</sup> oxidation state, while doping Cu atoms in the core region of QDs can lead to both Cu<sup>+1</sup> and Cu<sup>+2</sup> oxidation states, depending on the local environment of Cu atoms in the QDs. In addition, it is found that the optical absorption of the Cu-doped Cd<sub>33</sub>Se<sub>33</sub> QD in the visible region is mainly affected by Cu concentration, while the absorption in the infrared regime is closely related to the oxidation state of Cu. The present results enable us to use the doping of Cu impurity in CdSe QDs to achieve special photophysical properties for their applications in high-efficiency photovoltaic devices. The methods used here to resolve the electronic and optical properties of Cu-doped CdSe QDs can be extended to other II-VI semiconductor QDs incorporating transition-metal ions with variable valence.

**Keywords:** DFT; CdSe quantum dots; oxidation state of Cu; doping; optical absorption



**Citation:** Zhao, F.; Hu, S.; Xu, C.; Xiao, H.; Zhou, X.; Zu, X.; Peng, S. Effect of Copper Doping on Electronic Structure and Optical Absorption of Cd<sub>33</sub>Se<sub>33</sub> Quantum Dots. *Nanomaterials* **2021**, *11*, 2531. <https://doi.org/10.3390/nano11102531>

Academic Editor: Marc Cretin

Received: 6 September 2021

Accepted: 23 September 2021

Published: 28 September 2021

**Publisher's Note:** MDPI stays neutral with regard to jurisdictional claims in published maps and institutional affiliations.



**Copyright:** © 2021 by the authors. Licensee MDPI, Basel, Switzerland. This article is an open access article distributed under the terms and conditions of the Creative Commons Attribution (CC BY) license (<https://creativecommons.org/licenses/by/4.0/>).

## 1. Introduction

Doping of semiconductor nanocrystals (NCs) or quantum dots (QDs) with transition-metal ions has attracted significant interest in the applications of lasers [1,2], biolabeling [3–6], light-emitting diodes [7–9], and optoelectronics devices [10–14]. In particular, the transition-metal ions that can introduce permanent, electrically, or optically active charges are desired dopants [2,15,16]. The active charge can be permanently introduced into the NC host lattice by incorporating a transition-metal ion having a variable valence [17,18]. By such doping, new energy levels could be introduced into the bandgap of the host NCs, which can exchange charges with the valence band or the conduction band, thereby significantly influence their electronic and optical properties. Copper exhibits variable valences (+1 and +2) and has become a promising doping element in II-VI semiconductor NCs to modify the electronic and optical properties for their desirable applications [2,17,19–21].

Several studies have been devoted to the incorporation of Cu impurity in II-VI semiconductor NCs (e.g., CdSe, CdS, and ZnSe) to introduce copper-related intragap emission property [18,22–25]. However, some questions still exist on the origin of dopant emission in these Cu-doped NCs. In materials such as CdSe NCs, a model system for studying the electronic and photophysical properties of doped II-VI semiconductor NCs [15,26–30], there is still disagreement on the oxidation state of Cu ion whether it presents a +1 or +2 valence state. Meulenberg et al. used soft X-ray absorption near-edge spectroscopy (XANES), X-ray photoelectron spectroscopy (XPS), and photoluminescence (PL) to examine

the electronic and chemical structures of Cu ions dispersed in CdSe QDs and concluded that Cu ions had a +1 oxidation state [29]. The same +1 oxidation state for Cu in CdSe NCs was also assumed in Refs. [21,31]. However, Viswanatha et al. reported that Cu impurities in ZnSe/CdSe core-shell NCs exhibited a +2 oxidation state and served as a permanent source of optically active holes [17]. Brovelli et al. claimed that although the photoluminescence from their ZnSe/CdSe core-shell QDs was mainly attributed to Cu<sup>2+</sup> ions, the possibility that some QDs might contain Cu<sup>+</sup> ions could not be excluded [18]. To date, it is still unclear whether the oxidation state of Cu depends on its spatial distribution in CdSe QDs. This is mainly due to the difficulty of incorporating a well-controlled number of dopants at precise positions in small QDs. Therefore, it is important to understand the effects of the dopant environment on the photophysical properties of small-sized QDs. The second question is the location of Cu 3d orbitals within the forbidden band of II-VI NCs. Several research groups have reported that Cu 3d states were just above the valence band [24,32,33], while others claimed that Cu 3d orbitals were close to the conduction band [34]. The different positions of Cu 3d energy levels within the forbidden band will lead to very different recombination mechanisms of Cu impurity emission [32,35]. Thus far, it is unknown how the position of Cu 3d states varies with the dopant location in QDs either. Therefore, it is critical to investigate how the location of dopants in QDs influences the local atomic structure of QDs and thus modifies the state of Cu 3d orbitals as well as the optical properties of QDs.

To explore how the location of Cu dopants (at the surface or in the core region) affects the oxidation state of Cu ions and the position of Cu 3d orbitals in the energy levels of the Cu-doped semiconductor nanocrystals, we conduct a systematic density functional theory (DFT)-based study of the structural, energetic, electronic, and optical properties on the Cu-containing CdSe QDs. The Heyd-Scuseria-Ernzerhof (HSE) screened Coulomb hybrid functional was used in our DFT calculations, which is well known to predict the correct bandgaps of a wide range of materials successfully [36–38]. Wurtzite-based Cd<sub>33</sub>Se<sub>33</sub> nanocluster with a core-cage structure was used as the host NC in this work, which has been experimentally demonstrated to be extremely stable and used as a model system for the II-VI semiconductor nanocrystals [30]. Previous extensive theoretical studies have been conducted focusing on its special atomic arrangement [39–42]. Therefore, the Cd<sub>33</sub>Se<sub>33</sub> is a suitable host nanocrystal for the incorporation of copper impurity. Here, up to three Cu atoms are doped to substitute Cd atoms at different locations of a Cd<sub>33</sub>Se<sub>33</sub> QD. Details of the dopant locations are described in the Methodologies Section. The corresponding structural distortions, energetics, electronic properties, and optical absorption spectra were investigated, respectively. The present work provides a theoretical perspective on how to control Cu dopants in CdSe NCs to achieve desired optoelectronic properties for their applications in high-efficiency photovoltaic devices.

## 2. Methodologies

All calculations were carried out based on the density functional theory (DFT) implemented in the Vienna ab initio simulation package (VASP) [43]. The ion-electron interactions were treated by the projector augmented-wave (PAW) approach [44,45]. The exchange-correction effects were described by the screened hybrid functional of HSE with a mixed approach combining Hartree-Fock (HF) and Perdew-Burke-Ernzerhof (PBE) [44]. Here, an HF:GGA mixing ratio of 0.33 and a range-separation parameter of 0.15 Å<sup>-1</sup> were used, which successfully predicted the lattice parameters and bandgap for bulk wurtzite CdSe. The HSE setup was used for all the CdSe QDs in this work. A 1 × 1 × 1 Monkhorst-Pack mesh in the Brillouin zone was set for all CdSe QDs. Plane-wave cutoff energy of 350 eV was used, which resulted in good convergence of the total energy. To prevent spurious interactions between a QD and its periodic images, a vacuum spacing of at least 16 Å between the QD and its replicas was used in the simulation cells.

The Cd<sub>33</sub>Se<sub>33</sub> was constructed on the basis of bulk wurtzite (WZ) lattice with a Cd-Se bond distance of 2.688 Å. Similar construction methods for modeling CdSe quantum

dots have been widely used in previous publications [39–42]. In the unrelaxed  $\text{Cd}_{33}\text{Se}_{33}$  (Figure 1), the wurtzite core was formed by stacking two  $\text{Cd}_3\text{Se}_3$  rings (so the core is  $\text{Cd}_6\text{Se}_6$ ), which were enclosed by the Cd-terminated and Se-terminated surface facets, respectively. The definition of Cd or Se termination followed that in Ref [41]. The non-core atoms were treated as surface atoms. It should be noted that the core and surface of a nanocrystal can be distinguished in experiments [39,46]. In the core region, a Cu dopant binds to four adjacent Se atoms before relaxation, which is the same as in a bulk CdSe. On the surface, a Cu dopant has two to four nearest Se atoms before relaxation. In the case of the core doping, Cu dopants can be close to the Cd or Se termination or both. Therefore, the incorporation of Cu atoms into the core region is divided into three cases: a Cu dopant substituting a Cd atom near the Cd-terminated facet is defined as type I substitution in the core region (marked as “ $\text{C}_I$ ”); a Cu dopant replacing a Cd atom near the Se-terminated facet is defined as the type II substitution in the core region (denoted as “ $\text{C}_{II}$ ”); a Cu dopant near the Cd-terminated and the other near the Se-terminated is defined as type III substitution in the core region (marked as “ $\text{C}_{III}$ ”). As for the surface substitution (S), all Cd sites on the surface were tested for Cu doping, and the lowest energy site was selected for further study.

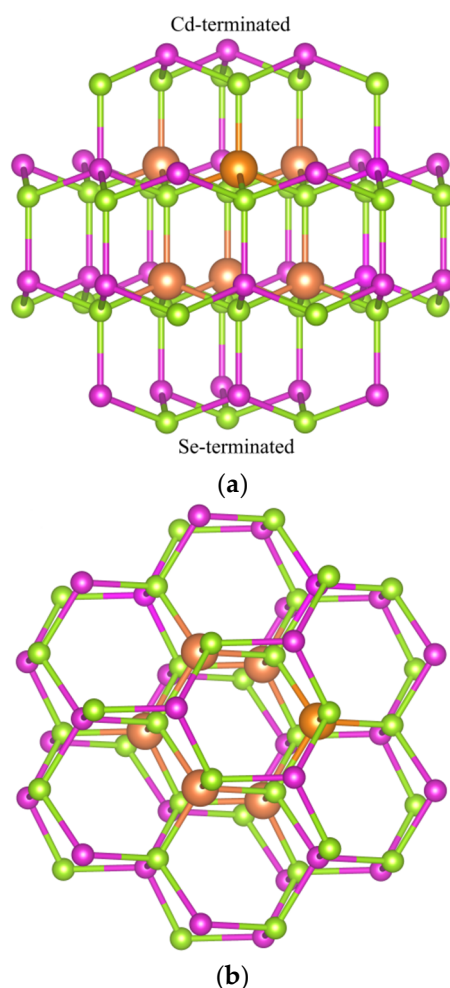


**Figure 1.** Geometrical structures of the unrelaxed  $\text{Cd}_{33}\text{Se}_{33}$  quantum dots: (a) side view of the  $\text{Cd}_{33}\text{Se}_{33}$  with the Se-terminated (bottom) and Cd-terminated (top) facets; (b) top view of  $\text{Cd}_{33}\text{Se}_{33}$ . The candidate doping sites (Cd sites) for a Cu impurity are labeled by small purple spheres for surface sites and large orange spheres for core sites, respectively; the Se atoms are represented by green spheres.

### 3. Results and Discussion

#### 3.1. Geometry Distortions of Cu-Doped Cd<sub>33</sub>Se<sub>33</sub> Quantum Dots

After relaxation, the wurtzite core structure is retained in both pristine and Cu-doped Cd<sub>33</sub>Se<sub>33</sub> QDs, although the surface structure has some degree of reconstruction. The average Se-Cd bond length in the relaxed pristine QD is determined to be 2.667 Å located between 2.678 Å in the core region and 2.657 Å in the surface region, which agree well with the value of 2.685 Å in other DFT calculations [39]. These values are slightly smaller than the Cd-Se bond length of 2.688 Å in bulk wurtzite CdSe, suggesting the lattice contraction effect in the nanocrystal. To further analyze the local environment for Cu atoms in Cd<sub>33</sub>Se<sub>33</sub> QDs, the <Cu-Se> bond distance and <Se-Cu-Se> bond angles are summarized in Table 1 and graphically presented in Figure 2. For comparison, the <Cd-Se> bond distances and <Se-Cd-Se> bond angles in the pristine Cd<sub>33</sub>Se<sub>33</sub> are also presented. It is found that the value of d<Cd-Se> in the pristine Cd<sub>33</sub>Se<sub>33</sub> is larger than those of d<Cu-Se> in Cu-doped QDs, meaning that Cu doping results in shorter distances between a substituting site (Cd-site) and its neighboring Se atoms. This phenomenon may be attributed to the larger ionic radius of Cd than that of Cu [47]. The optimized Cu-Se bonds on the surface of the QD are about 6–8% shorter than those in the core, as indicated in Table 1 and Figure 2a. The 6–8% deviation is greater than the 0.8% difference between the core and surface region in Cd-Se bonds, indicating that the surface Cu induces a significant surface reconstruction. For the bond angle (∠), the ∠Se-Cu-Se between a Cu atom and its adjacent Se atoms in Cu-doped Cd<sub>33</sub>Se<sub>33</sub> QDs are calculated in Table 1. The Se-Cd-Se bond angles in the core and surface regions for pristine Cd<sub>33</sub>Se<sub>33</sub> (denoted as Cd<sub>33</sub>Se<sub>33</sub> (C) and Cd<sub>33</sub>Se<sub>33</sub> (S), respectively) are also presented, where Cd atom is the one replaced by Cu. The Se-Cu-Se bond angle in Cu-doped Cd<sub>33</sub>Se<sub>33</sub> (C) QDs ranging from 109.85° to 120.0° is generally larger than the original Se-Cd-Se bond angle of 109.04° in pristine Cd<sub>33</sub>Se<sub>33</sub> QD, indicating the inward relaxation of Cu atoms in the core region. The phenomenon is similar to the case of Ag in CdSe QDs [48]. The <Se-Cd-Se> bond angle is calculated to be around 109.5° (sp<sup>3</sup>-like bond feature), and the coordination of substituted atoms (Cd atoms) in the core region of Cd<sub>33</sub>Se<sub>33</sub> QDs is four. When a Cu atom incorporates into the core region, the coordination of substituted atoms became four-coordinated upon relaxation since <Se-Cu-Se> bond angles are around 120° (sp<sup>2</sup> bond character). As for two Cu atoms incorporated in the core region, the distribution of <Se-Cu-Se> bond angles is similar to the case of <Se-Cd-Se> bond angles in Cd<sub>33</sub>Se<sub>33</sub> (C), suggesting that the coordination of substituted atoms does not change after Cu atoms incorporation. However, in the surface-doped QDs, Cu dopants are finally bonded to two Se atoms after relaxation with the <Se-Cu-Se> bond angles ranging from 168.5° to 177.83° as shown in Table 1, which are different from <Se-Cu-Se> bond angles of 119.78° in surface-doped Cd<sub>33</sub>Se<sub>33</sub> QDs. These differences in Cu-Se bonds (or <Se-Cu-Se> bond angles) of the surface and core region before and after Cu incorporation indicate that Cu doping in the QDs induces significant structural reconstruction.

**Table 1.** The Cu-Se bond length (d<Cu-Se>) and Se-Cu-Se bond angle (∠Se-Cu-Se) between a Cu atom and its adjacent Se atoms in Cu-doped Cd<sub>33</sub>Se<sub>33</sub> QDs. The Cd-Se bond length (d<Cd-Se>) in the core region (denoted as “C”), and Se-Cd-Se bond angle (∠Se-Cd-Se) in the surface region (denoted as “S”) for pristine Cd<sub>33</sub>Se<sub>33</sub> are also presented as references, where Cd atom is the one replaced by Cu. The C<sub>I</sub>, C<sub>II</sub>, and C<sub>III</sub> are defined in Methodologies.

	d<Cd-Se> (Å)	d<Cu-Se> (Å)	∠Se-Cd-Se (°)	∠Se-Cu-Se (°)
Cd <sub>33</sub> Se <sub>33</sub> (C)	2.678		109.04	
Cd <sub>33</sub> Se <sub>33</sub> (S)	2.657		119.78	
CuCd <sub>32</sub> Se <sub>33</sub> (S)		2.262		177.83
Cu <sub>2</sub> Cd <sub>31</sub> Se <sub>33</sub> (S)		2.269		171.93
Cu <sub>3</sub> Cd <sub>30</sub> Se <sub>33</sub> (S)		2.272		168.50
CuCd <sub>32</sub> Se <sub>33</sub> (C <sub>I</sub> )		2.414		120.0
CuCd <sub>32</sub> Se <sub>33</sub> (C <sub>II</sub> )		2.385		119.8
Cu <sub>2</sub> Cd <sub>31</sub> Se <sub>33</sub> (C <sub>I</sub> )		2.442		113.28
Cu <sub>2</sub> Cd <sub>31</sub> Se <sub>33</sub> S (C <sub>I</sub> )		2.477		109.39
Cu <sub>2</sub> Cd <sub>31</sub> Se <sub>33</sub> (C <sub>II</sub> )		2.522		109.85
Cu <sub>2</sub> Cd <sub>31</sub> Se <sub>33</sub> S (C <sub>II</sub> )		2.486		104.85
Cu <sub>2</sub> Cd <sub>31</sub> Se <sub>33</sub> (C <sub>III</sub> )		2.451		112.51

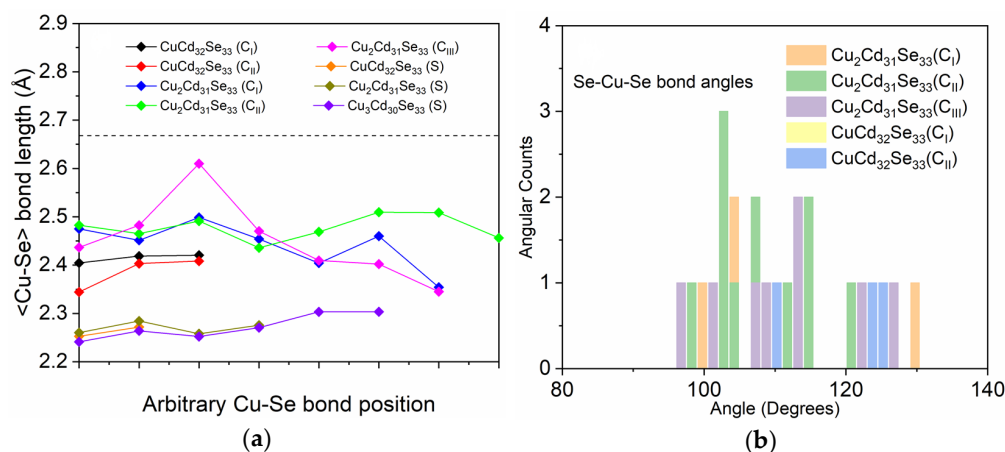


**Figure 2.** (a) The Cu-Se bond length in Cu-doped Cd<sub>33</sub>Se<sub>33</sub> quantum dots, together with the Cd-Se bond length in pristine Cd<sub>33</sub>Se<sub>33</sub> as indicated by the dashed line; (b) the bond-angle distributions of Se-Cu-Se when Cu atoms are doped in the core region of Cd<sub>33</sub>Se<sub>33</sub>.

### 3.2. Stability of Cu-Doped Cd<sub>33</sub>Se<sub>33</sub> QDs

To investigate the stability of Cu dopants in Cd<sub>33</sub>Se<sub>33</sub> QDs, the binding energy ( $E_b$ ) per Cu atom is calculated by using the following Equation [49]:

$$E_b = \left[ \left( E_{\text{undoped}} + nE_{\text{Cu}} \right) - \left( E_{\text{doped}} + nE_{\text{Cd}} \right) \right] / n$$

Here,  $E_{\text{undoped}}$  and  $E_{\text{doped}}$  are the total energies of the Cd<sub>33</sub>Se<sub>33</sub> and Cu-doped Cd<sub>33</sub>Se<sub>33</sub> QDs, respectively;  $E_{\text{Cd}}$  and  $E_{\text{Cu}}$  are the total energies per atom in bulk Cd and Cu, respectively;  $n$  is the number of Cu dopants. The binding energy per Cu atom and total dopant binding energy are presented in Table 2. Similar to [22], here, a positive binding energy means that Cu is energetically favorable to replace Cd; meanwhile, a larger binding energy means that the Cu dopant has a stronger tendency to bind with the CdSe QDs. As shown in Table 2, the Cu binding energy decreases with the increasing number of Cu atoms for both surface- and core-doped Cd<sub>33</sub>Se<sub>33</sub>, meaning that the stability of the system decreases as Cu content increases. When three Cu atoms are introduced in Cd<sub>33</sub>Se<sub>33</sub>, the binding energy becomes negative. This result suggests that the number of doped Cu atoms in Cd<sub>33</sub>Se<sub>33</sub> should be less than three per QD to maintain the system stability. In terms of Cu dopants at different locations of Cd<sub>33</sub>Se<sub>33</sub>, incorporation of one Cu atom at the surface (CuCd<sub>32</sub>Se<sub>33</sub> (S)) generally results in a larger binding energy than that in the core region (CuCd<sub>32</sub>Se<sub>33</sub> (C<sub>I</sub>) and CuCd<sub>32</sub>Se<sub>33</sub> (C<sub>II</sub>)), suggesting that a Cu dopant prefers to segregate to the surface. For doping two Cu atoms, Cu<sub>2</sub>Cd<sub>31</sub>Se<sub>33</sub> (C<sub>III</sub>) has a larger binding energy than the surface-doped Cu<sub>2</sub>Cd<sub>31</sub>Se<sub>33</sub> (S), while Cu<sub>2</sub>Cd<sub>31</sub>Se<sub>33</sub> (C<sub>I</sub>) and Cu<sub>2</sub>Cd<sub>31</sub>Se<sub>33</sub> (C<sub>II</sub>) exhibit smaller binding energies, compared to Cu<sub>2</sub>Cd<sub>31</sub>Se<sub>33</sub> (S). As discussed in the next section, these differences originate from the different oxidation states of Cu dopants in Cd<sub>33</sub>Se<sub>33</sub> QDs. The results also demonstrate that the location and concentration of Cu atoms play important roles in system stability.

### 3.3. Oxidation State for Cu Dopants in Cd<sub>33</sub>Se<sub>33</sub> Quantum Dots

Generally, Cu<sup>+</sup> has a fully filled 3d<sup>10</sup> electron shell and exhibits non-magnetic properties, whereas Cu<sup>2+</sup> has one unpaired electron in their 3d<sup>9</sup> shell and thus behaves paramagnetically [17,18]. In our calculations, when Cu dopants are incorporated on the surface, the spin-up and spin-down states are symmetric for the Cu 3d orbitals (Figure 3a), indicative of a non-magnetic character. Therefore, Cu dopants in surface-doped Cd<sub>33</sub>Se<sub>33</sub> present the +1 oxidation state. When one or two Cd sites in the QD core are replaced by Cu, the Cu 3d orbitals show distinct electronic features for different substitution locations, as presented in Figure 3b–f. In the case of doping a Cu atom in the core regardless near the Cd-terminated or Se-terminated surface (CuCd<sub>32</sub>Se<sub>33</sub> (C<sub>I</sub>) or CuCd<sub>32</sub>Se<sub>33</sub> (C<sub>II</sub>)), as shown

in Figure 3b–c), the density of states (DOS) of the Cu 3d states shows similar symmetric characters as those of surface-doped one ( $\text{CuCd}_{32}\text{Se}_{33}(\text{S})$ ), indicating that the +1 oxidation state of Cu is presented in these systems. The Cu 3d orbitals in  $\text{Cu}_2\text{Cd}_{31}\text{Se}_{33}(\text{C}_{\text{III}})$  (where one Cu dopant is close to the Cd termination and the other is near the Se termination) also show non-magnetic DOS distributions and thus the  $\text{Cu}^+$  electronic character, as shown in Figure 3f. However, when both Cu dopants are near the Cd termination ( $\text{Cu}_2\text{Cd}_{31}\text{Se}_{33}(\text{C}_{\text{I}})$ ) or Se termination ( $\text{Cu}_2\text{Cd}_{31}\text{Se}_{33}(\text{C}_{\text{II}})$ ), the spin-up and spin-down states are asymmetric, as shown in Figure 3d–e. Such electronic characters indicate that the systems contain some magnetism, which further indicates the oxidation state of Cu is  $\text{Cu}^{2+}$ . It should be noted that the Cu impurity energy levels in both  $\text{Cu}_2\text{Cd}_{31}\text{Se}_{33}(\text{C}_{\text{I}})$  and  $\text{Cu}_2\text{Cd}_{31}\text{Se}_{33}(\text{C}_{\text{II}})$  reside about 0.43 eV and 0.46 eV above from the valence band maximum (which is very close to the Fermi level), respectively. These impurity levels correspond to the lower half of the forbidden gap (i.e.,  $E_{\text{g}/2} = 0.93$  eV and 1.12 eV, where  $E_{\text{g}}$  is bandgap) indicative of p-type dopants, which is evidence for the +2 oxidation state of Cu [18]. In addition, the behavior of  $\text{Cu}^{2+}$  orbitals in our calculations is similar to the experimental observation of  $\text{Cu}^{2+}$  level in Cu-doped ZnSe NCs in which it was in the bandgap about 0.3–0.4 eV above the top of the valence band [50]. To further analyze the oxidation state of Cu in the QD, Bader charge calculations are performed for all Cu-doped  $\text{Cd}_{33}\text{Se}_{33}$ . A positive value of a Bader charge means the loss of electrons; otherwise, it means the gain of electrons. As shown in Table 3, the charge state of Cu ions in  $\text{Cu}_2\text{Cd}_{31}\text{Se}_{33}(\text{C}_{\text{I}})$  and  $\text{Cu}_2\text{Cd}_{31}\text{Se}_{33}(\text{C}_{\text{II}})$  is about 0.084–0.129 |e| more positive than that for Cu ions in  $\text{CuCd}_{32}\text{Se}_{33}(\text{S})$ ,  $\text{CuCd}_{32}\text{Se}_{33}(\text{C}_{\text{I}})$ ,  $\text{CuCd}_{32}\text{Se}_{33}(\text{C}_{\text{II}})$ , and  $\text{Cu}_2\text{Cd}_{31}\text{Se}_{33}(\text{C}_{\text{III}})$ , suggesting that Cu ions lose more electrons in  $\text{Cu}_2\text{Cd}_{31}\text{Se}_{33}(\text{C}_{\text{I}})$  and  $\text{Cu}_2\text{Cd}_{31}\text{Se}_{33}(\text{C}_{\text{II}})$  than in other cases. This is consistent with that the oxidation state of  $\text{Cu}^{2+}$  in  $\text{Cu}_2\text{Cd}_{31}\text{Se}_{33}(\text{C}_{\text{I}})$  and  $\text{Cu}_2\text{Cd}_{31}\text{Se}_{33}(\text{C}_{\text{II}})$  is larger than the oxidation state of  $\text{Cu}^{1+}$  in other CdSe QDs.

**Table 2.** The total binding energy of Cu atoms and the binding energy per Cu atom for Cu in  $\text{Cd}_{33}\text{Se}_{33}$ . The location where Cd atoms are substituted by Cu is indicated in the parenthesis. The S,  $\text{C}_{\text{I}}$ ,  $\text{C}_{\text{II}}$ , and  $\text{C}_{\text{III}}$  are defined in Methodologies.

	Total Binding Energy (eV)	Binding Energy/Cu Atom (eV)
$\text{CuCd}_{32}\text{Se}_{33}(\text{S})$	1.824	1.824
$\text{CuCd}_{32}\text{Se}_{33}(\text{C}_{\text{I}})$	1.726	1.726
$\text{CuCd}_{32}\text{Se}_{33}(\text{C}_{\text{II}})$	1.466	1.466
$\text{Cu}_2\text{Cd}_{31}\text{Se}_{33}(\text{S})$	0.538	0.269
$\text{Cu}_2\text{Cd}_{31}\text{Se}_{33}(\text{C}_{\text{I}})$	0.267	0.134
$\text{Cu}_2\text{Cd}_{31}\text{Se}_{33}(\text{C}_{\text{II}})$	0.497	0.248
$\text{Cu}_2\text{Cd}_{31}\text{Se}_{33}(\text{C}_{\text{III}})$	0.797	0.398
$\text{Cu}_3\text{Cd}_{30}\text{Se}_{33}(\text{S})$	−0.397	−0.466

**Table 3.** Average Bader charge (|e|) for each ion in Cu-doped  $\text{Cd}_{33}\text{Se}_{33}$  QDs. The S,  $\text{C}_{\text{I}}$ ,  $\text{C}_{\text{II}}$  and  $\text{C}_{\text{III}}$  are defined in Methodologies.

	Cu	Cd	Se
$\text{CuCd}_{32}\text{Se}_{33}(\text{S})$	0.204	0.647	−0.634
$\text{CuCd}_{32}\text{Se}_{33}(\text{C}_{\text{I}})$	0.288	0.671	−0.660
$\text{CuCd}_{32}\text{Se}_{33}(\text{C}_{\text{II}})$	0.261	0.671	−0.659
$\text{Cu}_2\text{Cd}_{31}\text{Se}_{33}(\text{S})$	0.266	0.673	−0.648
$\text{Cu}_2\text{Cd}_{31}\text{Se}_{33}(\text{C}_{\text{I}})$	0.345	0.674	−0.654
$\text{Cu}_2\text{Cd}_{31}\text{Se}_{33}(\text{C}_{\text{II}})$	0.390	0.670	−0.653
$\text{Cu}_2\text{Cd}_{31}\text{Se}_{33}(\text{C}_{\text{III}})$	0.287	0.670	−0.647
$\text{Cu}_3\text{Cd}_{30}\text{Se}_{33}(\text{S})$	0.260	0.667	−0.630

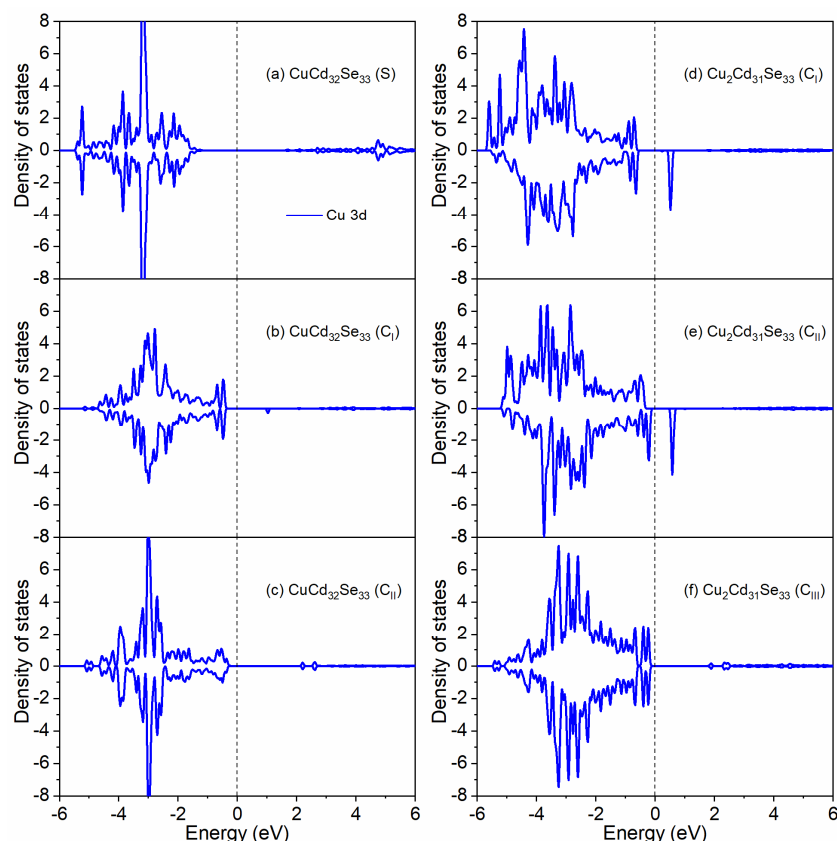


**Figure 3.** Orbital projected density of state (DOS) for Cu 3d in (a)  $\text{CuCd}_{32}\text{Se}_{33}$  (S); (b)  $\text{CuCd}_{32}\text{Se}_{33}$  ( $\text{C}_I$ ); (c)  $\text{CuCd}_{32}\text{Se}_{33}$  ( $\text{C}_{II}$ ); (d)  $\text{Cu}_2\text{Cd}_{31}\text{Se}_{33}$  ( $\text{C}_I$ ); (e)  $\text{Cu}_2\text{Cd}_{31}\text{Se}_{33}$  ( $\text{C}_{II}$ ); (f)  $\text{Cu}_2\text{Cd}_{31}\text{Se}_{33}$  ( $\text{C}_{III}$ ). Here, only the case of  $\text{CuCd}_{32}\text{Se}_{33}$  (S) is presented since the spin-up and spin-down states of the Cu 3d orbitals are symmetric for all the surface-doped  $\text{Cu}:\text{Cd}_{33}\text{Se}_{33}$ . The Fermi level is located at 0 eV.

Combined with the calculated binding energy in Section 3.2, it seems that the system with  $\text{Cu}^+$  ions ( $\text{CuCd}_{32}\text{Se}_{33}$  (S),  $\text{CuCd}_{32}\text{Se}_{33}$  ( $\text{C}_I$ ),  $\text{CuCd}_{32}\text{Se}_{33}$  ( $\text{C}_{II}$ ),  $\text{Cu}_2\text{Cd}_{31}\text{Se}_{33}$  ( $\text{C}_{III}$ ), and  $\text{Cu}_2\text{Cd}_{31}\text{Se}_{33}$  (S)) is more stable than that with  $\text{Cu}^{2+}$  impurity ions ( $\text{Cu}_2\text{Cd}_{31}\text{Se}_{33}$  ( $\text{C}_{II}$ )) because the former has larger binding energies than the later (Table 2). Our results are consistent with previous studies in which the oxidation state of Cu (+1) is more stable than Cu (+2) in some ZnS and CdS hosts [32,51].

### 3.4. Electronic Properties for Cu-Doped $\text{Cd}_{33}\text{Se}_{33}$ Quantum Dots

To explore how Cu impurity influences the electronic structure of  $\text{Cd}_{33}\text{Se}_{33}$ , the density of states with and without Cu dopants are presented in Figure 4 for surface doping and Figure 5 for core doping, respectively. For the pristine  $\text{Cd}_{33}\text{Se}_{33}$  (Figure 4a), previously we have demonstrated [48] that the mid-gap states primarily consist of Se 4p orbitals locating above the valence band (VB); the conduction band is mainly composed of Cd 5s and Se 4p states. With one Cu dopant incorporated into the surface (Figure 4b), the mid-gap states, which mainly consist of Se 4p states from two-coordinated surface Se atoms, are located on the top of the valence band. The Cu 3d orbitals in the VB are located about 1.35 eV below the Fermi level so that they do not contribute to the mid-gap states. In the forbidden band, a new Se 4p impurity state above Fermi level emerges. With the increasing Cu dopants on the surface (Figure 4c), the mid-gap states above the VB disappear and Cu 3d orbitals shift toward the top of the valence band. The impurity levels still exist in the forbidden gap but shift toward the conduction band minimum.

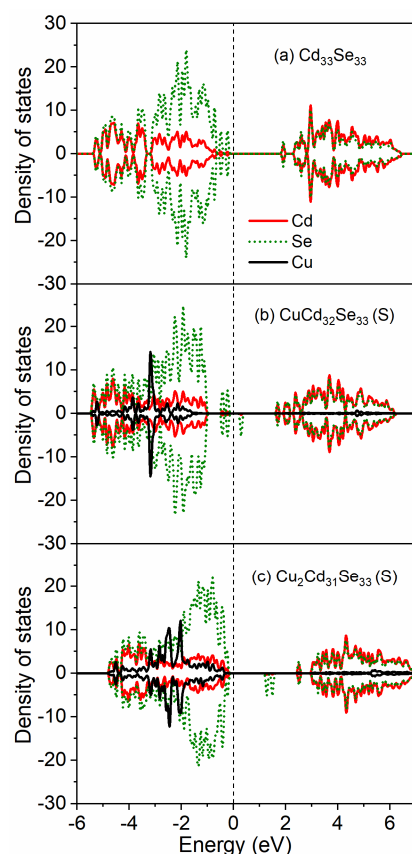


**Figure 4.** Projected density of states (DOS) for each type of ion when Cu atoms are doped at the surface of  $\text{Cd}_{33}\text{Se}_{33}$ : (a) pristine  $\text{Cd}_{33}\text{Se}_{33}$ ; (b)  $\text{CuCd}_{32}\text{Se}_{33}$  (S); (c)  $\text{Cu}_2\text{Cd}_{31}\text{Se}_{33}$  (S). The Fermi level is located at 0 eV.

The incorporation of Cu dopants into the core region (Figure 5) results in very different electronic structures from those on the surface, but these doped NCs still maintain the insulating character. Such an insulating character for core-doped  $\text{Cu}:\text{Cd}_{33}\text{Se}_{33}$  is in drastic contrast to the metallic-like character for core-doped  $\text{Ag}:\text{Cd}_{33}\text{Se}_{33}$  in which some electrons are located at the Fermi level of the system [48]. In  $\text{CuCd}_{32}\text{Se}_{33}$  ( $C_I$ ) shown in Figure 5b, the mid-gap states consisting of mainly Se 4p orbitals and slightly Cu 3d orbitals are just located above the valence band. Hybridization of Cu 3d orbitals with Se 4p states appears above the VB and both of them contribute to the mid-gap states. Similar hybridization electronic states above the VB have been also observed when a Cu impurity replaces a central Cd atom in zinc-blende-based CdSe NCs (note our NCs are based on the Wurtzite structure), although they consist of Cu 3d orbitals primarily [52]. The energy levels of dopant d orbitals are deeper than the anion p states in VB showing the “inverted” bonding character in  $\text{CuCd}_{32}\text{Se}_{33}$  ( $C_I$ ). This is different from the “normal” bonding feature (in which the dopant d orbitals are located at shallower energy levels than the anion p states in VB) for a Cu impurity locating on the center of a zinc blende (ZB) based CdSe nanocrystal [52]. When two Cu dopants are incorporated into the core region near the Cd-terminated ( $\text{Cu}_2\text{Cd}_{31}\text{Se}_{33}$  ( $C_I$ )) shown in Figure 5d, the mid-gap states are still above the VB but without the contribution from Cu 3d orbitals. However, as the Cu dopants are close to the Se-terminated ( $\text{CuCd}_{32}\text{Se}_{33}$  ( $C_{II}$ ) and  $\text{Cu}_2\text{Cd}_{31}\text{Se}_{33}$  ( $C_{II}$ )), the mid-gap states disappear, as can be seen in Figure 5c,e. More interestingly, when Cu dopants are near both Se-terminated and Cd-terminated in  $\text{Cu}_2\text{Cd}_{31}\text{Se}_{33}$  ( $C_{III}$ ), the mid-gap states with the hybridization of Cu 3d and Se 4p orbitals appear above the VB (Figure 5f). As for the conduction band of core-doped  $\text{Cu}:\text{Cd}_{33}\text{Se}_{33}$  QDs, an impurity level consisting of Se 4p states locates within the forbidden band in  $\text{CuCd}_{32}\text{Se}_{33}$  ( $C_I$ ) (Figure 5b) and  $\text{CuCd}_{32}\text{Se}_{33}$  ( $C_{II}$ ) (Figure 5c). With the increasing Cu dopants, an additional impurity level composed

of Cu 3d orbitals appears within the forbidden band for  $\text{Cu}_2\text{Cd}_{31}\text{Se}_{33}$  ( $\text{C}_I$ ) (Figure 5d) and  $\text{Cu}_2\text{Cd}_{31}\text{Se}_{33}$  ( $\text{C}_{II}$ ) (Figure 5e). This is consistent with the electronic character of  $\text{Cu}^{2+}$  as described in Section 3.4. However, in the case of  $\text{Cu}_2\text{Cd}_{31}\text{Se}_{33}$  ( $\text{C}_{III}$ ) (Figure 5f), there are no impurity levels. The above electronic structure analysis demonstrates that the energy levels and shapes of the valence and conduction bands can be modified by changing Cu concentrations and locations in CdSe QDs, which will, in turn, affect the optical absorption properties of these QDs as discussed in the next section.

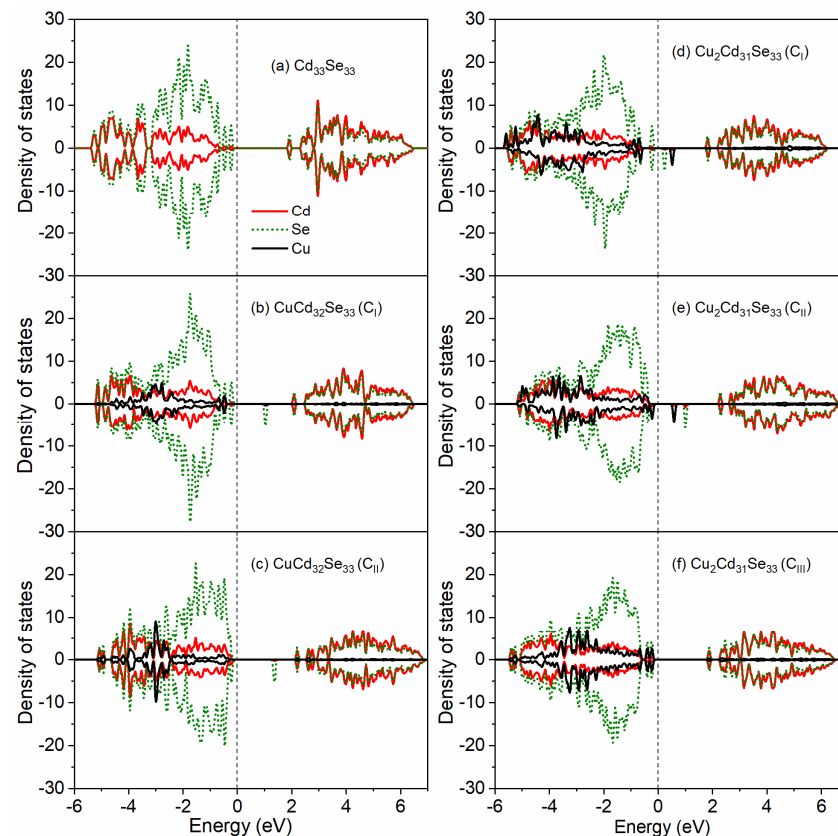


**Figure 5.** Projected density of states (DOS) for each type of ion when Cu atoms are doped in core region of  $\text{Cd}_{33}\text{Se}_{33}$ : (a) pristine  $\text{Cd}_{33}\text{Se}_{33}$ ; (b)  $\text{CuCd}_{32}\text{Se}_{33}$  ( $\text{C}_I$ ); (c)  $\text{CuCd}_{32}\text{Se}_{33}$  ( $\text{C}_{II}$ ); (d)  $\text{Cu}_2\text{Cd}_{31}\text{Se}_{33}$  ( $\text{C}_I$ ); (e)  $\text{Cu}_2\text{Cd}_{31}\text{Se}_{33}$  ( $\text{C}_{II}$ ); (f)  $\text{Cu}_2\text{Cd}_{31}\text{Se}_{33}$  ( $\text{C}_{III}$ ). The Fermi level is located at 0 eV.

### 3.5. Optical Absorption Spectra for Cu-Doped $\text{Cd}_{33}\text{Se}_{33}$ Quantum Dots

To explore how the copper incorporation affects the optical properties of  $\text{Cd}_{33}\text{Se}_{33}$  QDs, the optical absorption spectra of  $\text{Cd}_{33}\text{Se}_{33}$  with and without Cu dopants are calculated within the independent-particle approximation, which is known to provide a qualitative agreement of dielectric response functions between theory and experiment while neglecting self-energy, excitonic and local-field effects in the optical response [53,54]. For the  $\text{Cd}_{33}\text{Se}_{33}$  QD, the calculated lowest absorption peak is in good agreement with the experiments [30,55]. Clearly, doping of Cu in the  $\text{Cd}_{33}\text{Se}_{33}$  leads to different absorption spectra from the pristine one, as can be seen in Figure 6. In the visible region (the main figure of Figure 6), just one Cu dopant induces high-intensity absorption peaks in the range of 408–502 nm for  $\text{CuCd}_{32}\text{Se}_{33}$  (S), 380–428 nm for  $\text{CuCd}_{32}\text{Se}_{33}$  ( $\text{C}_I$ ), and 445–574 nm for  $\text{CuCd}_{32}\text{Se}_{33}$  ( $\text{C}_{II}$ ). In experiments, the enhancement of absorption spectra in the wavelength range between 390 and 600 nm was also observed in Cu-doped CdSe NCs [19,22,31]. When two or three Cu atoms are doped, absorption peaks are relatively weaker within the same wavelength range. These results indicate that the optical intensity of Cu-doped  $\text{Cd}_{33}\text{Se}_{33}$  in the visible region strongly correlates with Cu dopant content. A similar dopant-concentration-dependent trend in optical

absorption was also observed in Ag-doped CdSe QDs [48]. These new absorption features result predominantly from the electronic transition from Se 4p orbitals in the valence band to Se 4p and Cd 5s states in the conduction band (as shown in Figures 4 and 5).

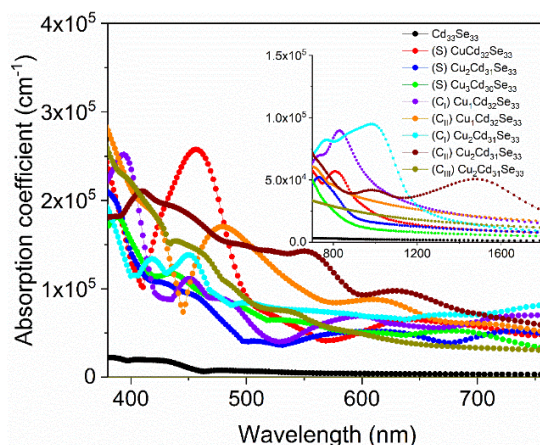


**Figure 6.** Absorption coefficients as a function of wavelength for  $\text{Cd}_{33}\text{Se}_{33}$  QDs without and with Cu doping in the visible region in the main figure. The inset shows the absorption coefficients of these QDs in the infrared region.

In the infrared regime (displayed in the inset of Figure 6), the  $\text{Cu}_2\text{Cd}_{31}\text{Se}_{33}$  ( $\text{C}_I$ ) exhibits a stronger absorption peak than other CdSe QDs between 815 and 1161 nm; The  $\text{Cu}_2\text{Cd}_{31}\text{Se}_{33}$  ( $\text{C}_{II}$ ) has a unique absorption peak from 1148 to 1777 nm. These absorption features are induced mainly by electronic excitations from Se 4p orbitals on the top of VB to Cu 3d orbitals in the forbidden gap (as indicated in Figure 5). As analyzed in Section 3.4, Cu dopants show the +2 oxidation state in  $\text{Cu}_2\text{Cd}_{31}\text{Se}_{33}$  ( $\text{C}_I$ ) and  $\text{Cu}_2\text{Cd}_{31}\text{Se}_{33}$  ( $\text{C}_{II}$ ) while exhibiting the +1 oxidation state in other QDs. The result indicates that incorporation of  $\text{Cu}^{2+}$  in  $\text{Cd}_{33}\text{Se}_{33}$  QDs can cause stronger optical absorption in the infrared regime than  $\text{Cu}^+$ . This can be explained by the fact that the 3d states of  $\text{Cu}^{2+}$  reside above the Fermi level and are near the valence band edge (Figure 5d,e). Such an electronic structure can lead to a small sub-bandgap electronic transition from VB to impurity levels and thus enhance optical absorption in the long-wavelength range.

Our results suggest that the incorporation of Cu can dramatically enhance the optical absorption of  $\text{Cd}_{33}\text{Se}_{33}$  QD within the visible regime and extend the absorption edges into the infrared regime. Furthermore, the optical absorption of Cu-doped  $\text{Cd}_{33}\text{Se}_{33}$  in the visible regime is affected mainly by Cu dopant concentration, while the absorption in the infrared regime is closely related to the oxidation state of Cu.

#### 4. Conclusions

In this work, a systematic density functional theory (DFT) modeling using the Heyd–Scuseria–Ernzerhof (HSE) screened Coulomb hybrid functional was conducted to explore how the location and concentration of Cu dopants influence the structural, energetic, electronic, and optical properties of a magic-sized  $\text{Cd}_{33}\text{Se}_{33}$  QD. It was found that the oxidation state of Cu dopants is closely related to their substitution location and concentration. Doping of Cu at the surface of  $\text{Cd}_{33}\text{Se}_{33}$  QD leads to the  $\text{Cu}^+$  3d orbitals distributions. Similar distributions of  $\text{Cu}^+$  3d states were also observed for Cu in the core region such as  $\text{CuCd}_{32}\text{Se}_{33}$  ( $\text{C}_I$ ) (Cu atom near the Cd-terminated),  $\text{CuCd}_{32}\text{Se}_{33}$  ( $\text{C}_{II}$ ) (Cu atom near the Se-terminated), and  $\text{Cu}_2\text{Cd}_{31}\text{Se}_{33}$  ( $\text{C}_{III}$ ) (one Cu atom near the Cd-terminated and the other near the Se-terminated). However, doping of both copper atoms at internal Cd-sites near Cd-terminated or Se-terminated leads to the  $\text{Cu}^{2+}$  electronic character. Further binding energy calculations showed that in general, the Cu dopants with a +1 oxidation state are energetically more stable than those with a +2 oxidation state in  $\text{Cd}_{33}\text{Se}_{33}$ . It was also found that the optical absorption coefficient of Cu-doped  $\text{Cd}_{33}\text{Se}_{33}$  in the infrared regime

is closely related to the oxidation state of Cu rather than Cu concentration. On the other hand, doping of only one Cu atom introduces stronger absorption peaks than the doping of two Cu atoms in the range of 380–574 nm, indicating that the absorption coefficient is sensitive to Cu concentration in the visible regime. This work demonstrates that the dopant location and concentration can have significant effects on the electronic structure of Cu 3d states. Therefore, the proper control of the dopant concentration and position is critical for improving the efficiency and performance of CdSe QD-based optoelectronic devices.

**Author Contributions:** Conceptualization, F.Z. and S.P.; methodology, F.Z. and S.H.; validation, F.Z. and C.X.; investigation, H.X., X.Z. (Xiaosong Zhou), X.Z. (Xiaotao Zu); writing—original draft preparation, F.Z.; writing—review and editing, S.H., C.X., H.X., X.Z. (Xiaosong Zhou) and X.Z. (Xiaotao Zu); supervision, S.P. All authors have read and agreed to the published version of the manuscript.

**Funding:** This work is partially supported by a funded project by the China Postdoctoral Science Foundation (2021TQ0312), the National Key Research and Development Program of China (2017YFE0301600, 2016YFB0201203), and the President Foundation of CAEP (YZJLX2018003).

**Institutional Review Board Statement:** Not applicable.

**Informed Consent Statement:** Not applicable.

**Data Availability Statement:** The data presented in this study are available on request from the corresponding author. The data are not publicly available due to ethical.

**Acknowledgments:** The calculations were performed at the National Supercomputing Center at Wuxi and Shanghai Supercomputer Center.

**Conflicts of Interest:** The authors declare no conflict of interest.

## References

1. Klimov, V.I.; Ivanov, S.A.; Nanda, J.; Achermann, M.; Bezel, I.; McGuire, J.A.; Piryatinski, A. Single-Exciton Optical Gain in Semiconductor Nanocrystals. *Nature* **2007**, *447*, 441–446. [[CrossRef](#)] [[PubMed](#)]
2. Mocatta, D.; Cohen, G.; Schattner, J.; Millo, O.; Rabani, E.; Banin, U. Heavily Doped Semiconductor Nanocrystal Quantum Dots. *Science* **2011**, *332*, 77–81. [[CrossRef](#)] [[PubMed](#)]
3. Mattoussi, H.; Mauro, J.M.; Goldman, E.R.; Anderson, G.P.; Sundar, V.C.; Mikulec, F.V.; Bawendi, M.G. Self-Assembly of CdSe–ZnS Quantum Dot Bioconjugates Using an Engineered Recombinant Protein. *J. Am. Chem. Soc.* **2000**, *122*, 12142–12150. [[CrossRef](#)]
4. Mattoussi, H.; Mauro, J.; Goldman, E.; Green, T.; Anderson, G.; Sundar, V.; Bawendi, M. Bioconjugation of Highly Luminescent Colloidal CdSe–ZnS Quantum Dots with an Engineered Two-Domain Recombinant Protein. *Phys. Status Solidi B* **2001**, *224*, 277–283. [[CrossRef](#)]
5. Santra, S.; Yang, H.; Holloway, P.H.; Stanley, J.T.; Mericle, R.A. Synthesis of Water-Dispersible Fluorescent, Radio-Opaque, and Paramagnetic CdS:Mn/ZnS Quantum Dots: A Multifunctional Probe for Bioimaging. *J. Am. Chem. Soc.* **2005**, *127*, 1656–1657. [[CrossRef](#)]
6. Pradhan, N.; Battaglia, D.M.; Liu, Y.; Peng, X. Efficient, Stable, Small, and Water-Soluble Doped ZnSe Nanocrystal Emitters as Non-Cadmium Biomedical Labels. *Nano Lett.* **2007**, *7*, 312–317. [[CrossRef](#)]
7. Wood, V.; Halpert, J.E.; Panzer, M.J.; Bawendi, M.G.; Bulović, V. Alternating Current Driven Electroluminescence from ZnSe/ZnS:Mn/ZnS Nanocrystals. *Nano Lett.* **2009**, *9*, 2367–2371. [[CrossRef](#)] [[PubMed](#)]
8. Janßen, N.; Whitaker, K.M.; Gamelin, D.R.; Bratschitsch, R. Ultrafast Spin Dynamics in Colloidal ZnO Quantum Dots. *Nano Lett.* **2008**, *8*, 1991–1994. [[CrossRef](#)]
9. Yang, H.; Holloway, P.H.; Ratna, B.B. Photoluminescent and Electroluminescent Properties of Mn-Doped ZnS Nanocrystals. *J. Appl. Phys.* **2003**, *93*, 586–592. [[CrossRef](#)]
10. Warkentin, M.; Bridges, F.; Carter, S.A.; Anderson, M. Electroluminescence Materials ZnS:Cu,Cl and ZnS:Cu,Mn,Cl Studied by EXAFS Spectroscopy. *Phys. Rev. B* **2007**, *75*, 075301. [[CrossRef](#)]
11. Smith, B.A.; Zhang, J.Z.; Joly, A.; Liu, J. Luminescence Decay Kinetics of Mn<sup>2+</sup>-Doped ZnS Nanoclusters Grown in Reverse Micelles. *Phys. Rev. B* **2000**, *62*, 2021–2028. [[CrossRef](#)]
12. Lu, W.; Gao, P.; Jian, W.B.; Wang, Z.L.; Fang, J. Perfect Orientation Ordered In-Situ One-Dimensional Self-Assembly of Mn-Doped PbSe Nanocrystals. *J. Am. Chem. Soc.* **2004**, *126*, 14816–14821. [[CrossRef](#)]
13. Norberg, N.S.; Parks, G.L.; Salley, G.M.; Gamelin, D.R. Giant Excitonic Zeeman Splittings in Colloidal Co<sup>2+</sup>-Doped ZnSe Quantum Dots. *J. Am. Chem. Soc.* **2006**, *128*, 13195–13203. [[CrossRef](#)] [[PubMed](#)]
14. Fainblat, R.; Barrows, C.J.; Gamelin, D.R. Single Magnetic Impurities in Colloidal Quantum Dots and Magic-Size Clusters. *Chem. Mater.* **2017**, *29*, 8023–8036. [[CrossRef](#)]

15. Sahu, A.; Kang, M.S.; Kompch, A.; Notthoff, C.; Wills, A.W.; Deng, D.; Winterer, M.; Frisbie, C.D.; Norris, D.J. Electronic Impurity Doping in CdSe Nanocrystals. *Nano Lett.* **2012**, *12*, 2587–2594. [[CrossRef](#)]
16. Chen, D.; Viswanatha, R.; Ong, G.L.; Xie, R.; Balasubramanian, M.; Peng, X. Temperature Dependence of “Elementary Processes” in Doping Semiconductor Nanocrystals. *J. Am. Chem. Soc.* **2009**, *131*, 9333–9339. [[CrossRef](#)]
17. Viswanatha, R.; Brovelli, S.; Pandey, A.; Crooker, S.A.; Klimov, V.I. Copper-Doped Inverted Core/Shell Nanocrystals with “Permanent” Optically Active Holes. *Nano Lett.* **2011**, *11*, 4753–4758. [[CrossRef](#)] [[PubMed](#)]
18. Brovelli, S.; Galland, C.; Viswanatha, R.; Klimov, V.I. Tuning Radiative Recombination in Cu-Doped Nanocrystals via Electrochemical Control of Surface Trapping. *Nano Lett.* **2012**, *12*, 4372–4379. [[CrossRef](#)]
19. Dutta, A.; Bera, R.; Ghosh, A.; Patra, A. Ultrafast Carrier Dynamics of Photo-Induced Cu-Doped CdSe Nanocrystals. *J. Phys. Chem. C* **2018**, *122*, 16992–17000. [[CrossRef](#)]
20. Ning, J.; Liu, J.; Levi-Kalisman, Y.; Frenkel, A.I.; Banin, U. Controlling Anisotropic Growth of Colloidal ZnSe Nanostructures. *J. Am. Chem. Soc.* **2018**, *140*, 14627–14637. [[CrossRef](#)] [[PubMed](#)]
21. Yang, L.; Knowles, K.E.; Gopalan, A.; Hughes, K.E.; James, M.C.; Gamelin, D.R. One-Pot Synthesis of Monodisperse Colloidal Copper-Doped CdSe Nanocrystals Mediated by Ligand–Copper Interactions. *Chem. Mater.* **2016**, *28*, 7375–7384. [[CrossRef](#)]
22. Alperson, B.; Rubinstein, I.; Hodes, G. Identification of Surface States on Individual CdSe Quantum Dots by Room-Temperature Conductance Spectroscopy. *Phys. Rev. B* **2001**, *63*, 081303. [[CrossRef](#)]
23. Jana, S.; Srivastava, B.B.; Acharya, S.; Santra, P.K.; Jana, N.R.; Sarma, D.D.; Pradhan, N. Prevention of Photooxidation in Blue–Green Emitting Cu Doped ZnSe Nanocrystals. *Chem. Commun.* **2010**, *46*, 2853. [[CrossRef](#)] [[PubMed](#)]
24. Mandal, P.; Talwar, S.S.; Major, S.S.; Srinivasa, R.S. Orange-Red Luminescence from Cu Doped CdS Nanophosphor Prepared Using Mixed Langmuir–Blodgett Multilayers. *J. Chem. Phys.* **2008**, *128*, 114703. [[CrossRef](#)] [[PubMed](#)]
25. Pradhan, N.; Goorskey, D.; Thessing, J.; Peng, X. An Alternative of CdSe Nanocrystal Emitters: Pure and Tunable Impurity Emissions in ZnSe Nanocrystals. *J. Am. Chem. Soc.* **2005**, *127*, 17586–17587. [[CrossRef](#)]
26. Xie, F.; Xie, R.; Wang, Q. Synthesis and Characterization of CuIn(S<sub>x</sub>Se<sub>1-x</sub>)<sub>2</sub> Nanocrystals. *Adv. Sci. Lett.* **2011**, *4*, 3624–3628. [[CrossRef](#)]
27. Buonsanti, R.; Milliron, D.J. Chemistry of Doped Colloidal Nanocrystals. *Chem. Mater.* **2013**, *25*, 1305–1317. [[CrossRef](#)]
28. Luo, H.; Tuinenga, C.; Guidez, E.B.; Lewis, C.; Shipman, J.; Roy, S.; Aikens, C.M.; Chikan, V. Synthesis and Characterization of Gallium-Doped CdSe Quantum Dots. *J. Phys. Chem. C* **2015**, *119*, 10749–10757. [[CrossRef](#)]
29. Meulenberg, R.W.; van Buuren, T.; Hanif, K.M.; Willey, T.M.; Strouse, G.F.; Terminello, L.J. Structure and Composition of Cu-Doped CdSe Nanocrystals Using Soft X-Ray Absorption Spectroscopy. *Nano Lett.* **2004**, *4*, 2277–2285. [[CrossRef](#)]
30. Kasuya, A.; Sivamohan, R.; Barnakov, Y.A.; Dmitruk, I.M.; Nirasawa, T.; Romanyuk, V.R.; Kumar, V.; Mamykin, S.V.; Tohji, K.; Jeyadevan, B.; et al. Ultra-Stable Nanoparticles of CdSe Revealed from Mass Spectrometry. *Nat. Mater.* **2004**, *3*, 99–102. [[CrossRef](#)]
31. Whitham, P.J.; Knowles, K.E.; Reid, P.J.; Gamelin, D.R. Photoluminescence Blinking and Reversible Electron Trapping in Copper-Doped CdSe Nanocrystals. *Nano Lett.* **2015**, *15*, 4045–4051. [[CrossRef](#)]
32. Corrado, C.; Jiang, Y.; Oba, F.; Kozina, M.; Bridges, F.; Zhang, J.Z. Synthesis, Structural, and Optical Properties of Stable ZnS:Cu,Cl Nanocrystals. *J. Phys. Chem. A* **2009**, *113*, 3830–3839. [[CrossRef](#)] [[PubMed](#)]
33. Srivastava, B.B.; Jana, S.; Pradhan, N. Doping Cu in Semiconductor Nanocrystals: Some Old and Some New Physical Insights. *J. Am. Chem. Soc.* **2011**, *133*, 1007–1015. [[CrossRef](#)] [[PubMed](#)]
34. Isarov, A.V.; Chrysochoos, J. Optical and Photochemical Properties of Nonstoichiometric Cadmium Sulfide Nanoparticles: Surface Modification with Copper(II) Ions. *Langmuir* **1997**, *13*, 3142–3149. [[CrossRef](#)]
35. Lilhare, D.; Sinha, T.; Khare, A. Influence of Cu Doping on Optical Properties of (Cd–Zn)S Nanocrystalline Thin Films: A Review. *J. Mater. Sci. Mater. Electron.* **2018**, *29*, 688–713. [[CrossRef](#)]
36. Harb, M.; Masih, D.; Takanebe, K. Screened Coulomb Hybrid DFT Investigation of Band Gap and Optical Absorption Predictions of CuVO<sub>3</sub>, CuNbO<sub>3</sub> and Cu<sub>5</sub>Ta<sub>11</sub>O<sub>30</sub> Materials. *Phys. Chem. Chem. Phys.* **2014**, *16*, 18198–18204. [[CrossRef](#)]
37. Deák, P.; Aradi, B.; Frauenheim, T.; Janzén, E.; Gali, A. Accurate Defect Levels Obtained from the HSE06 Range-Separated Hybrid Functional. *Phys. Rev. B* **2010**, *81*, 153203. [[CrossRef](#)]
38. Heyd, J.; Scuseria, G.E.; Ernzerhof, M. Hybrid Functionals Based on a Screened Coulomb Potential. *J. Chem. Phys.* **2003**, *118*, 8207–8215. [[CrossRef](#)]
39. Kilina, S.; Ivanov, S.; Tretiak, S. Effect of Surface Ligands on Optical and Electronic Spectra of Semiconductor Nanoclusters. *J. Am. Chem. Soc.* **2009**, *131*, 7717–7726. [[CrossRef](#)]
40. Kuznetsov, A.E.; Beratan, D.N. Structural and Electronic Properties of Bare and Capped Cd<sub>33</sub>Se<sub>33</sub> and Cd<sub>33</sub>Te<sub>33</sub> Quantum Dots. *J. Phys. Chem. C* **2014**, *118*, 7094–7109. [[CrossRef](#)]
41. Puzder, A.; Williamson, A.J.; Zaitseva, N.; Galli, G.; Manna, L.; Alivisatos, A.P. The Effect of Organic Ligand Binding on the Growth of CdSe Nanoparticles Probed by Ab Initio Calculations. *Nano Lett.* **2004**, *4*, 2361–2365. [[CrossRef](#)]
42. Puzder, A.; Williamson, A.J.; Gygi, F.; Galli, G. Self-Healing of CdSe Nanocrystals: First-Principles Calculations. *Phys. Rev. Lett.* **2004**, *92*, 217401. [[CrossRef](#)] [[PubMed](#)]
43. Hafner, J. ChemInform Abstract: Ab-Initio Simulations of Materials Using VASP: Density-Functional Theory and Beyond. *J. Comput. Chem.* **2008**, *29*, 2044–2078. [[CrossRef](#)] [[PubMed](#)]
44. Perdew, J.P.; Burke, K.; Ernzerhof, M. Generalized Gradient Approximation Made Simple. *Phys. Rev. Lett.* **1996**, *77*, 3865–3868. [[CrossRef](#)]

45. Perdew, J.P.; Burke, K.; Wang, Y. Generalized Gradient Approximation for the Exchange-Correlation Hole of a Many-Electron System. *Phys. Rev. B* **1996**, *54*, 16533–16539. [[CrossRef](#)]
46. Winkler, U.; Eich, D.; Chen, Z.H.; Fink, R.; Kulkarni, S.K.; Umbach, E. Detailed Investigation of CdS Nanoparticle Surfaces by High-Resolution Photoelectron Spectroscopy. *Chem. Phys. Lett.* **1999**, *306*, 95–102. [[CrossRef](#)]
47. Shannon, R.D. Revised Effective Ionic Radii and Systematic Studies of Interatomic Distances in Halides and Chalcogenides. *Acta Cryst. A* **1976**, *32*, 751–767. [[CrossRef](#)]
48. Zhao, F.A.; Xiao, H.Y.; Bai, X.M.; Zu, X.T. Effects of Ag Doping on the Electronic and Optical Properties of CdSe Quantum Dots. *Phys. Chem. Chem. Phys.* **2019**, *21*, 16108–16119. [[CrossRef](#)] [[PubMed](#)]
49. Suyver, J.F.; van der Beek, T.; Wuister, S.F.; Kelly, J.J.; Meijerink, A. Luminescence of Nanocrystalline ZnSe:Cu. *Appl. Phys. Lett.* **2001**, *79*, 4222–4224. [[CrossRef](#)]
50. Ganesan, P.; Lakshmipathi, S. Influence of Dopants Cu, Ga, In, Hg on the Electronic Structure of Cd<sub>n</sub>S<sub>n</sub> (*n* = 6, 15) Clusters—a DFT Study. *RSC Adv.* **2016**, *6*, 93056–93067. [[CrossRef](#)]
51. Liu, J.; Zhao, Y.; Liu, J.; Wang, S.; Cheng, Y.; Ji, M.; Zhou, Y.; Xu, M.; Hao, W.; Zhang, J. From Cu<sub>2</sub>S Nanocrystals to Cu Doped CdS Nanocrystals through Cation Exchange: Controlled Synthesis, Optical Properties and Their p-Type Conductivity Research. *Sci. China Mater.* **2015**, *58*, 693–703. [[CrossRef](#)]
52. Nelson, H.D.; Hinterding, S.O.M.; Fainblat, R.; Creutz, S.E.; Li, X.; Gamelin, D.R. Mid-Gap States and Normal vs Inverted Bonding in Luminescent Cu<sup>+</sup>- and Ag<sup>+</sup>-Doped CdSe Nanocrystals. *J. Am. Chem. Soc.* **2017**, *139*, 6411–6421. [[CrossRef](#)] [[PubMed](#)]
53. Gajdoš, M.; Hummer, K.; Kresse, G.; Furthmüller, J.; Bechstedt, F.J.P.R.B. Linear optical properties in the projector-augmented wave methodology. *Phys. Rev. B* **2006**, *73*, 045112. [[CrossRef](#)]
54. Schmidt, W.G. Calculation of reflectance anisotropy for semiconductor surface exploration. *Phys. Status Sol. B* **2005**, *242*, 2751–2764. [[CrossRef](#)]
55. Kudera, S.; Zanella, M.; Giannini, C.; Rizzo, A.; Li, Y.; Gigli, G.; Cingolani, R.; Ciccarella, G.; Spahl, W.; Parak, W.J.; et al. Sequential Growth of Magic-Size CdSe Nanocrystals. *Adv. Mater.* **2007**, *19*, 548–552. [[CrossRef](#)]